General laws of the propagation of few-cycle optical pulses with orbital angular momentum in free space

Miguel A. Porras and Raúl García-Álvarez

Grupo de Sistemas Complejos, ETSIME, Universidad Politécnica de Madrid, Rios Rosas 21, 28003 Madrid, Spain

We conduct a theoretical study of the propagation of few-cycle ultrafast vortices (UFVs) carrying orbital angular momentum (OAM) in free space. Our analysis reveals much more complex temporal dynamics than that of few-cycle fundamental Gaussian-like beams, particularly when approaching the single-cycle regime and the magnitude of the topological charge l is high. The recently described lower bound $\sqrt{|l|}$ to the number of oscillations of UFVs with propagation-invariant temporal shape (isodiffracting UFVs) is found to hold on average also for UFVs of general type, with variations along the propagation direction above and below that bound, even vanishing locally. These variations are determined by the so-called Porras factor, or g_0 factor, characterizing the dependence of the Rayleigh distance of the spectral constituents with frequency. With a given available bandwidth, UFVs must widen temporally with increasing magnitude of the topological charge and must widen or may shrink temporally during propagation as a result of the axially varying g_0-dependent lower bound. Under very restrictive conditions in their generation, an UFV can be shrunk below the lower bound $\sqrt{|l|}$ at a focus into a kind of locally compressed state of OAM, but it broadens well above $\sqrt{|l|}$ and is distorted in a tiny fraction of the depth of focus because of the dispersions introduced by Gouy's phase and wave-front mismatch. These propagation phenomena have implications and should be taken into account in experiments and applications of UFVs, such as the generation of high harmonics and attosecond pulses with high OAM, or in OAM-based ultrafast communications systems, as well as in other areas of physics such as acoustics or electron waves.

I. INTRODUCTION

In recent years there has been a great deal of interest in the generation and application of ultrafast vortices (UFVs), or ultrashort pulses carrying orbital angular momentum (OAM), particularly those with few optical cycles approaching the single-cycle regime, and in their application to, e.g., high-harmonic and attosecond pulse generation, high-resolution imaging, and fast optical classical and quantum information processing. In an important part of the experiments the aim is to generate shorter and shorter vortices of better quality by eliminating undesirable effects such as topological charge and angular dispersions [1–13]. Technical improvements have made it possible to approach the single-cycle regime of durations and to reach two-digit topological charges of the vortices [10]. On the other hand, the use of these UFVs in strong-field light-matter interactions, as in high-harmonic and attosecond generation experiments [14–21], has led to the generation of UFVs of high topological charges, typically a few dozen, even exotic waves with fractional and time-varying topological charges [22,23]. Recent proposals [24] that mimic high-harmonic generation based on phase-only spatial light modulators allow for increased topological charge on demand.

Given these huge experimental efforts, somewhat surprising is the small amount of theoretical work on the propagation characteristics of UFVs [25–36], even in the *a priori* simplest situation of free-space propagation. A comprehensive theory of the propagation dynamics of UFVs, similar to that developed a few decades ago for fundamental few-cycle pulses without OAM [37–45] when the single-cycle regime was reached [46], is still pending.

Indeed, the propagation dynamics of UFVs differs in substantial aspects from that of fundamental pulses without OAM because of a strong coupling between the temporal and OAM degrees of freedom in the UFV, as reported in [30–34] for Laguerre-Gauss-type UFVs and in [34–36] for nondiffracting X-type vortices. The effects of this coupling remain small, but are observable, at low topological charges and/or many-cycle durations, but become large and dominate the propagation dynamics when the single-cycle and high-topological-charge regimes are approached.

These previous studies considered the so-called isodiffracting UFVs, characterized by a Rayleigh distance that is independent of the frequency of the monochromatic Laguerre-Gauss (LG) constituents. Isodiffracting UFVs play a central role in the theory of UFV propagation because they are the only UFVs whose pulse temporal shape do not change during propagation regardless of how short the pulse and how high the topological charge are, as pointed out in [30]. For these UFVs, Ref. [30] establishes a strong coupling between the pulse temporal shape at the bright ring surrounding the vortex singularity and the magnitude of the topological charge that settles an upper bound to the topological charge that an UFV of a certain number of oscillations can carry, and vice versa,

settles a lower bound $\sqrt{|l|}$ to the number of oscillations of an UFV of given magnitude of the topological charge $|l|$. As a result, an UFV synthesized with a certain bandwidth must increase its duration from that expected from its bandwidth when the imprinted topological charge is increased [31].

However, femtosecond laser sources that emit with frequency-independent Rayleigh distance seem to be more the exception than the rule [47–50] (see [51] for a possible exception). The dependence of the Rayleigh distance on frequency is characterized by the g_0 factor, first introduced in [44]. For ultrafast Gaussian beams, a small red or blue carrier frequency shift experienced during propagation is determined by its g_0 factor. More importantly, the g_0 factor determines the carrier-envelope phase distribution in the focal volume [44,52]. This is why the g_0 factor of the source has proved to be a crucial parameter in phase-sensitive light-matter interactions, as in [47,48] for electron photoemission and in [49] for electron acceleration with radially polarized pulses, since the outcome of experiments depends crucially on the g_0 factor of the source. Conversely, use of phase-sensitive interactions allow the measurement of the carrier-envelope phase focal map and from it to determine the g_0 factor of the source [47]. The value $g_0 = 0$ corresponds to the isodiffracting geometry in ultrafast Gaussian beams and UFVs. Hoff *et al.* [47] report average values $g_0 = -1.95$ and $g_0 = -1.2$ in two experiments with the same source but different tuning; Jolly [49] suggests that high-power lasers would be characterized by $g_0 \simeq 1$; measurements of the carrier-envelope phase in [50,51] using similar few-cycle Kerr-lens mode-locked Ti:sapphire lasers suggest that these sources would be characterized by $-1 < g_0 < 0$. Most of these measurements indicate significant variations of the Rayleigh distance with frequency.

In this paper we study the propagation (focusing) of UFVs of the LG type beyond the isodiffracting model and therefore those synthesized from actual femtosecond laser sources with g_0 factors different from zero. We do not intend to describe in detail the propagation features of the different types of UFVs, whose detailed description could be deferred to separate studies, but reveal general laws in the form of temporal-OAM couplings that affect all of them and underlie the different propagation phenomena observed numerically. For clarity, we often compare the phenomena found here with those already known in ultrafast Gaussian beams and isodiffracting UFVs. We find that the lower bound to the number of oscillations of the pulse at the bright ring proportional to $\sqrt{|l|}$ continues to hold for general UFVs, with upward and downward axial variations averaging in $\sqrt{|l|}$ or a higher value whose location is dictated by the g_0 factor of the source. Thus, as for isodiffracting UFVs, the duration of general UFVs increases compared to that expected from the available source bandwidth with increasing imprinted topological charge. Unlike ultrafast Gaussian beams and isodiffracting UFVs, the duration and shape of general UFVs change during propagation as a result of the axially varying lower bound, these variations being more pronounced as $|l|$ and $|g_0|$ are larger and approaching the single-cycle regime. At certain axial locations it is possible to decrease the number of oscillations below $\sqrt{|l|}$, but this is only feasible in practice with sources with $0 < g_0 \leqslant 1$ at the far field and sources with $-1 \leqslant g_0 < 0$ at the waist or focus; the optimum situation is the use of a source with

$g_0 = -1$. Even if it is possible to locally beat the $\sqrt{|l|}$ limit in a kind of compressed state of OAM, the UFV broadens to a number of oscillations well above $\sqrt{|l|}$ in a small fraction of the depth of focus because of the strong dispersive effects of Gouy's phase and wave-front mismatch in UFVs with $g_0 \neq 0$ and high topological charges.

II. PRELIMINARIES ON ULTRAFAST LAGUERRE-GAUSS VORTICES

We represent an UFV of topological charge l propagating in free space as the superposition

$$E(r, t', z)e^{il\varphi} = \frac{1}{\pi} \int_0^\infty \hat{E}(r, \omega, z)e^{-i\omega t'} d\omega e^{il\varphi} \quad (1)$$

of LG monochromatic light beams

$$\hat{E}(r, \omega, z) = \hat{a}(\omega) \frac{s(\omega)}{s(\omega, z)} \left[\frac{\sqrt{2}r}{s(\omega, z)} \right]^{|l|} e^{-r^2/s^2(\omega, z)}$$
$$\times e^{i[\omega r^2/2cR(\omega, z)]} e^{-i(|l|+1)\psi(\omega, z)} \quad (2)$$

of zero radial order (the only ones used in the cited experiments) and of the same charge l. In the above equations, $a(\omega)$ are generally complex-valued weights, z is the paraxial propagation direction, (r, z, φ) are cylindrical coordinates, $t' = t - z/c$ is the local time, and

$$s(\omega) = \sqrt{\frac{2z_R(\omega)c}{\omega}} \quad (3)$$

is the width at the waist, located at $z = 0$, of the fundamental Gaussian beam ($l = 0$) as a function of the Rayleigh distance $z_R(\omega)$ of each LG monochromatic constituent. One could specify $s(\omega)$ and determine from it the Rayleigh distance from the standard relation $z_R(\omega) = \omega s^2(\omega)/2c$, but the opposite is more appropriate since the g_0 factor is directly linked to the Rayleigh distance. Also,

$$s(\omega, z) = s(\omega)\sqrt{1 + \frac{z^2}{z_R^2(\omega)}} = \sqrt{\frac{2z_R(\omega)c}{\omega}} \sqrt{1 + \frac{z^2}{z_R^2(\omega)}} \quad (4)$$

is the Gaussian width at each distance, $R(\omega, z) = z + z_R^2(\omega)/z$ is the radius of curvature of the wave fronts, and $\psi(\omega, z) = \tan^{-1}[z/z_R(\omega)]$ is Gouy's phase of the fundamental Gaussian beam. The divergence angle at the far field can be evaluated from $\theta(\omega) = \sqrt{2c/\omega z_R(\omega)}$. Being limited to positive frequencies, the optical field E in (1) is the analytical signal complex representation of the real optical field Re$\{E\}$ [53].

We also consider the spatial distribution of pulse energy, energy density, or fluence, given by

$$\mathcal{E}(r, z) = \int_{-\infty}^{\infty} [\mathrm{Re}E(r, t', z)]^2 dt' = \frac{1}{2} \int_{-\infty}^{\infty} |E(r, t', z)|^2 dt'$$
$$= \frac{1}{\pi} \int_0^\infty |\hat{E}(r, \omega, z)|^2 d\omega, \quad (5)$$

which vanishes at the vortex center at $r = 0$ and at infinity for a localized field and then takes a maximum value at a certain radius $r_{\max}$ at each propagation distance, henceforth referred to as the radius $r_{\max}$ of the bright ring. The temporal shape of the pulse at this radius is particularly relevant in

experiments, especially those involving nonlinear propagation and interactions with matter.

The optical field in Eqs. (1) and (2) may be regarded as generated on a plane source at $z = 0$. Alternatively, and more closely related to current experiments, Eqs. (1) and (2) also represent the focused optical field in the Debye approximation (no focal shift) [44], with the focus at $z = 0$, when an ideal focusing element of focal length f, as a spherical or parabolic mirror, is illuminated by an input field in the form of a collimated UFV

$$E_L(r, t)e^{il\varphi} = \frac{1}{\pi} \int_0^\infty \hat{E}_L(r, \omega) e^{-i\omega t} d\omega \, e^{il\varphi} \quad (6)$$

made of the collimated monochromatic LG beams

$$\hat{E}_L(r, \omega)e^{il\varphi} = \hat{A}(\omega)\left[\frac{\sqrt{2}r}{S(\omega)}\right]^{|l|} e^{-r^2/S^2(\omega)} e^{il\varphi} \quad (7)$$

of Rayleigh distance $Z_R(\omega)$, Gaussian width $S(\omega) = \sqrt{2Z_R(\omega)c/\omega}$ on the focusing system, and divergence angle $\Theta(\omega) = \sqrt{2c/\omega Z_R(\omega)}$. We cannot pursue the sophisticated experimental techniques for the generation of vortices of femtosecond duration as in Eqs. (6) and (7), but the Rayleigh distance $Z_R(\omega)$ and the spectrum $\hat{A}(\omega)$ in these equations are closely related to the geometry and spectrum of the femtosecond laser source. The spectrum $\hat{A}(\omega)$ is characterized by a certain mean frequency

$$\omega_0 = \frac{\int_0^\infty |\hat{A}(\omega)|^2 \omega \, d\omega}{\int_0^\infty |\hat{A}(\omega)|^2 d\omega} \quad (8)$$

and corresponds in the time domain to a certain pulse shape

$$A(t) = \frac{1}{\pi} \int_0^\infty \hat{A}(\omega) e^{-i\omega t} d\omega \quad (9)$$

of a physically meaningful carrier frequency ω_0 if, according to the standard definition [46], the full width at half maximum (FWHM) of $|A(t)|^2$ comprises at least one carrier period $2\pi/\omega_0$. In the Debye approximation of focusing, the Rayleigh distance and spectra of the focused UFV and of the input UFV from the femtosecond source are related by [54]

$$z_R(\omega) = \frac{f^2}{Z_R(\omega)}, \quad \hat{a}(\omega) = -i\frac{f}{z_R(\omega)}\hat{A}(\omega). \quad (10)$$

For ulterior use, given a function $f(\omega)$ of frequency, we introduce the notation

$$\overline{f(\omega)} = \frac{\int_0^\infty |\hat{E}(r, \omega, z)|^2 f(\omega) d\omega}{\int_0^\infty |\hat{E}(r, \omega, z)|^2 d\omega} \quad (11)$$

for its mean value with the spectral density $|\hat{E}(r, \omega, z)|^2$ of the UFV, and for any function $g(t')$ of time, the notation

$$\overline{g(t')} = \frac{\int_{-\infty}^\infty |E(r, t', z)|^2 g(t') dt'}{\int_{-\infty}^\infty |E(r, t', z)|^2 dt'} \quad (12)$$

for its mean value with the intensity $|E(r, t', z)|^2$ of the UFV. Note that these mean values depend in general on r and z because $|\hat{E}(r, \omega, z)|^2$ and $|E(r, t', z)|^2$ depend on r and z [and because $f(\omega)$ and $g(t')$ may be functions of r and z too]. The variance of $f(\omega)$ is $\sigma_{f(\omega)}^2 = \overline{[f(\omega) - \overline{f(\omega)}]^2} = \overline{f^2(\omega)} - \overline{f(\omega)}^2$, and similarly for a function of time. In particular, $\bar{\omega}$

is the mean or carrier frequency at any point of the UFV and $\sigma_\omega^2 = \overline{\omega^2} - \bar{\omega}^2$ is the variance of ω with the spectral density. Similarly, $\overline{t'}$ is the mean temporal location and $\sigma_{t'}^2 = \overline{t'^2} - \overline{t'}^2$ is the variance of time with the pulse intensity. Suitable measures of the spectral bandwidth and duration of the UFV at a given point (r, z) are the so-called Gaussian-equivalent half-bandwidth and half-duration $\Delta\omega = 2\sigma_\omega$ and $\Delta t = 2\sigma_{t'}$, respectively, yielding the $1/e^2$-decay half-width for Gaussian spectral density and intensity. The product $\Delta t \Delta\omega$ is always larger than or equal to 2, with the minimum value of 2 reached for the Gaussian-shaped spectral density $|\hat{E}(r, \omega, z)|^2$ with uniform spectral phases. Also, the product $\bar{\omega}\Delta t/\pi = 2\Delta t/T$, where $T = 2\pi/\bar{\omega}$ is the mean or carrier period, is the number of oscillations in the full Gaussian-equivalent duration $2\Delta t$, but to avoid these π factors in relevant formulas we will refer to $\bar{\omega}\Delta t$ as the number of oscillations.

A. The g_0 factor of the source

In previous theoretical studies on UFVs, $Z_R(\omega)$, and hence $z_R(\omega)$, is taken to be independent of frequency in the isodiffracting model of UFVs, in which case the temporal shape of the UFV does not change with propagation distance. While this property confers on isodiffracting UFVs a prominent place from the theoretical point of view, current femtosecond laser sources emit pulses with different Rayleigh distances for different frequencies, as recently demonstrated [47,48]. Since the function $Z_R(\omega)$ is generally unknown, several simple models are often used [49]. For example, the model $Z_R(\omega) = Z_R(\omega_0)(\omega/\omega_0)^{g_0}$ yields, using the above relations between $Z_R(\omega)$, $S(\omega)$, and $\Theta(\omega)$, $S(\omega) = S(\omega_0)(\omega/\omega_0)^{(g_0-1)/2}$ and $\Theta(\omega) = \Theta(\omega_0)(\omega_0/\omega)^{(g_0+1)/2}$ for the input UFV, and using Eqs. (10), $z_R(\omega) = z_R(\omega_0)(\omega_0/\omega)^{g_0}$, $s(\omega) = s(\omega_0)(\omega_0/\omega)^{(g_0+1)/2}$, and $\theta(\omega) = \theta(\omega_0)(\omega/\omega_0)^{(g_0-1)2}$ for the focused UFV. In particular, $g_0 = 0$ is the isodiffracting model, $g_0 = 1$ describes an input UFV with constant width, and hence a focused UFV with constant convergence angle and focal width inversely proportional to frequency, and $g_0 = -1$ describes an input UFV with constant divergence angle and width inversely proportional to frequency, corresponding to a focused UFV with convergence angle inversely proportional to frequency and constant width at the focus. With other g_0 values, none of the parameters are constant. The above formula for $Z_R(\omega)$ is a simple model that will be used in the examples below, but obviously real sources do not have to conform to it.

Fortunately, for pulses with at least one carrier oscillation, it has been theoretically suggested and experimentally demonstrated that it is only the variation of the Rayleigh distance with frequency in the vicinity of the carrier frequency ω_0 that determines most of propagation properties of pulsed beams [44,47,52]. The different situations are suitably described by a single dimensionless parameter called the g_0 factor, defined as [44]

$$g_0 = \left.\frac{dZ_R(\omega)}{d\omega}\right|_{\omega_0} \frac{1}{Z_R(\omega_0)}\omega_0 = -\left.\frac{dz_R(\omega)}{d\omega}\right|_{\omega_0} \frac{1}{z_R(\omega_0)}\omega_0, \quad (13)$$

that characterizes the variation of the Rayleigh range with frequency about the carrier frequency ω_0. The symbol g_0 is
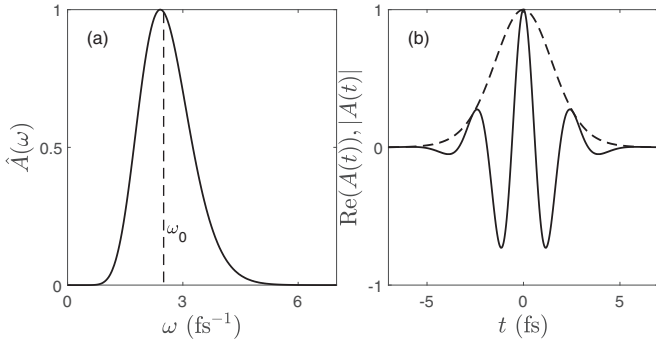
FIG. 1. Power-exponential spectrum $\hat{A}(\omega) \propto (\omega/\omega_0)^{\alpha-1/2}$ $\exp(-\alpha\omega/\omega_0)$ with $\alpha = 14.25$ and $\omega_0 = 2.5$ rad/fs of the quasi-Gaussian pulse $A(t) = [-i\alpha/(\omega_0 t - i\alpha)]^{\alpha+1/2}$ of carrier frequency ω_0. The value of α is chosen such that the FWHM duration of $|A(t)|^2$ is one carrier period. For $\alpha = 14.25$ or higher $\hat{A}(\omega)$ approaches a Gaussian spectrum but without a DC component at $\omega = 0$, and $A(t)$ approaches a Gaussian pulse, as detailed, e.g., in [41,55].

the same as in the model in the preceding paragraph because they coincide in that model. Thus, $g_0 = 1$ means constant width $S(\omega)$ only about ω_0, $g_0 = -1$ constant divergence about ω_0, and so on. Recent studies outline the need of measuring the g_0 factor for each particular femtosecond laser source since its value has been evidenced to strongly affect the outcome of experiments with these sources, particularly those involving phase-sensitive light-matter interactions [47–51]. Recent direct measurements yield values of g_0 between -1 and -2 for femtosecond sources using hollow-core fiber compressors [47]. High-power lasers are suggested to have $g_0 = +1$ [49], and the values inferred from measurements of the carrier-envelope phase of focused few-cycle pulses from Kerr-lens mode-locked Ti:sapphire lasers are in the range $-1 < g_0 < 0$ [50,51]. Thus, according to previous literature, we assume here that $|g_0|$ does not exceed 2.

B. Previous results and open problems

Figures 1 and 2 illustrate previously known results for Gaussian beams and for isodiffracting UFVs, compared with the phenomena in the propagation of general UFVs considered here. In all cases represented in Fig. 2, the source spectrum $\hat{A}(\omega)$, shown in Fig. 1(a), is the same and corresponds in time domain to the approximately Gaussian pulse $A(t)$ shown in Fig. 1(b) containing a single oscillation in the FWHM of $|A(t)|^2$. All the graphs in Fig. 2 represent pulse shapes ReE and amplitudes $|E|$ of focused UFVs at the radii r_{max} of maximum fluence at each propagation distance.

First, focusing of few-cycle, even single-cycle pulses in the form of a fundamental Gaussian beam [$l = 0$ in Eqs. (1) and (2) and $r_{max} = 0$] only introduces minor changes to the pulse temporal shape [Figs. 2(a)–2(c)], irrespective of the particular value of g_0, i.e., the pulse continues to be an approximately single-cycle Gaussian-like pulse during the whole propagation [42], with slightly blueshifted frequency for $g_0 > 0$ and redshifted frequency for $g_0 < 0$ about the

focus [38,39,44] and with different maps of carrier-envelope phase in the focal volume, as studied in detail in [44,52].

Second, with the same source spectrum in Fig. 1 of a single-cycle pulse, the number of oscillations of the synthesized isodiffracting input UFV ($g_0 = 0$) monotonically increases with the magnitude of the topological charge from that expected from the source pulse $A(t)$, no matter by what technical means it is generated, and the focused isodiffracting UFV maintains this temporal shape during the whole focusing process, with no appreciable blue or red frequency shift at the bright ring, $\bar{\omega} \simeq \omega_0$. The increase of the number of oscillations with $|l|$ is a consequence of the upper bound to the relative bandwidth $\sigma_\omega/\bar{\omega} < 1/\sqrt{|l|}$ at the bright ring described in [30] or on account of the relation $\Delta t \, \Delta\omega \geqslant 2$ ($\Delta\omega = 2\sigma$), the lower bound $\bar{\omega}\Delta t > \sqrt{|l|}$ to the number of oscillations [30]. In addition, with $\bar{\omega} \simeq \omega_0$ for isodiffracting UFV [34], $\Delta t > \sqrt{|l|}/\omega_0$ imposes directly a lower bound to the pulse duration. Thus, irrespective of how wide the source spectrum is or how short the source pulse $A(t)$ that can be synthesized with it is, the UFV adapts itself to a number of oscillations satisfying $\omega_0\Delta t > \sqrt{|l|}$ [31].

The intention of this paper is to understand propagation phenomena of UFVs with $g_0 \neq 0$, such as those observed in Figs. 2(g)–2(i). In this example $g_0 = 1$ because the width $S(\omega) \equiv S(\omega_0)$ of the input UFV is taken to be independent of frequency, and according to Eqs. (6) and (7) the input field is $E_L(r, t)e^{il\varphi} = A(t)[\sqrt{2}r/S(\omega_0)]^{|l|}e^{-r^2/S^2(\omega_0)}e^{il\varphi}$. First, unlike pulsed Gaussian beams and isodiffracting UFVs, the pulse shape at r_{max} changes during focusing. Pulse distortion is weak for small $|l|$ but quite pronounced for large $|l|$, as in Figs. 2(g)–2(i). Second, the topological charge and duration of the input UFV in Fig. 1(b) and its initial stage of focusing in Fig. 2(g) are chosen so that the inequality $\omega_0\Delta t > \sqrt{|l|}$ is violated, contradicting apparently the results in [30]. However, this lower bound applies only to the most fundamental situation of UFVs with propagation-invariant pulse shape. Indeed, there is no restriction, on physical grounds, to produce the space-time factorized field $E_L(r, t)e^{il\varphi} = A(t)[\sqrt{2}r/S(\omega_0)]^{|l|}e^{-r^2/S^2(\omega_0)}e^{il\varphi}$, with $A(t)$ as short and $|l|$ as large as desired at a given transversal plane only technical issues. About the focus, however, the UFV is distorted and broadened, as in Figs. 2(h) and 2(i), so the inequality $\bar{\omega}\Delta t > \sqrt{|l|}$ is satisfied by far. In the following sections we demonstrate that this behavior is a result of more general restrictions on the number of oscillations at the bright ring that generalize $\bar{\omega}\Delta t > \sqrt{|l|}$ for isodiffracting UFVs to general UFVs.

III. GENERAL RESTRICTIONS TO THE PULSE PROPERTIES AT THE BRIGHT RING

To that purpose we first locate the maximum of the fluence distribution at each transversal plane. Differentiating with respect to r, the fluence in Eq. (5) with the spectral density $|\hat{E}(r, \omega, z)|^2$ obtained from Eq. (2), we obtain, after some algebra,

$$\frac{d\mathcal{E}}{dr} = \frac{2}{r} \int_0^\infty d\omega |\hat{E}|^2 \left[|l| - \frac{2r^2}{s^2(\omega, z)} \right], \quad (14)$$
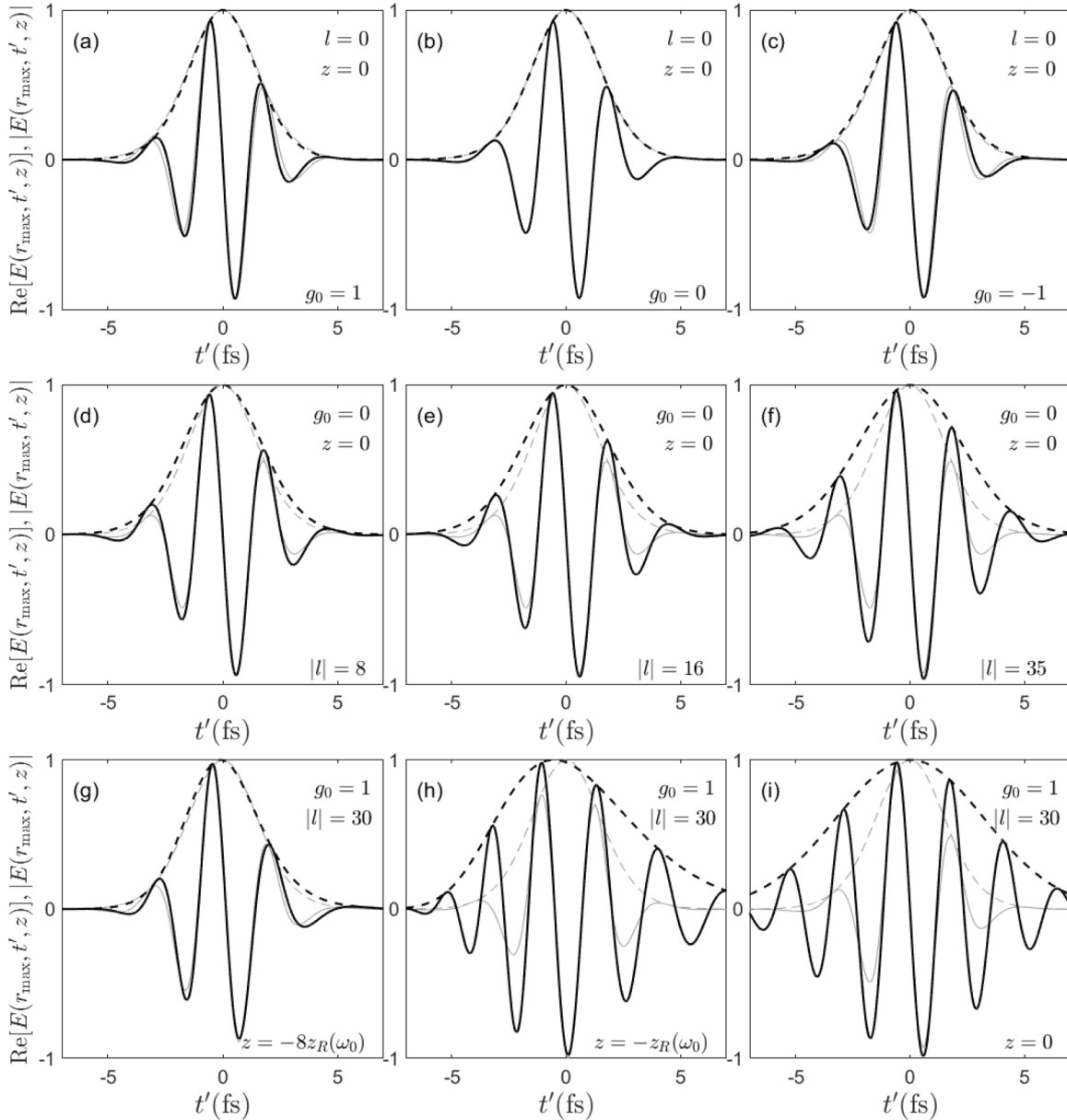
FIG. 2. Focused pulse shapes and amplitudes at the radius r_{max} of maximum fluence for a different input optical field of interest. All of them are evaluated numerically from Eqs. (1), (2), and (10) with $f = 20$ cm and with the same spectrum $\hat{A}(\omega)$ of the single-cycle pulse in Fig. 1 and using the model $Z_R(\omega) = Z_R(\omega_0)(\omega/\omega_0)^{g_0}$ with $Z_R(\omega_0) = 4$ m. Pulse shapes are shown at the focus for the fundamental pulsed Gaussian beam ($l = 0$) with the three choices (a) $g_0 = 1$, (b) $g_0 = 0$, and (c) $g_0 = -1$. All three are undistorted quasi-Gaussian pulses of the same duration during the whole propagation with slightly blueshifted ($g_0 = 1$) or redshifted frequencies ($g_0 = -1$) at the focus. Pulse shapes are shown at the focus in the isodiffracting model with $g_0 = 0$ and (d) $|l| = 8$, (e) $|l| = 16$, and (f) $|l| = 35$. All three propagate undistorted without any frequency shift but with duration increasing with $|l|$. Pulse shapes are shown for $g_0 = 1$ and $|l| = 30$ at different propagation distances: (g) $z = -8z_R(\omega_0)$, (h) $z = -z_R(\omega_0)$, and (i) $z = 0$. The pulse is slightly blueshifted, distorted, and broadened during focusing. The gray curves are always the pulse in Fig. 1(b) with an artificially added phase in each case for a better appreciation of the frequency shifts. In all figures the peak amplitude is set to unity and shifted to $t' = 0$ for a better comparison.

which equated to zero leads to the implicit equation

$$\frac{|l|}{2} = r_{max}^2 \overline{\left(\frac{1}{s^2(\omega, z)}\right)}(r_{max}) \tag{15}$$

for the maxima or minima of the fluence, where we have explicitly written that the (r, z)-dependent mean value $\overline{1/s^2(\omega, z)}$ is evaluated at the radius of r_{max} of the bright ring. Differentiating again with respect to r, the second derivative yields a

cumbersome and long expression, which evaluated again at r_{max} yields however the simpler expression

$$\left.\frac{d^2\mathcal{E}}{dr^2}\right|_{r_{max}} = -8\mathcal{E}(r_{max})\overline{\left(\frac{1}{s^2(\omega, z)}\right)}(r_{max})$$

$$\times \left[|l| + 1 - |l|\frac{\overline{1/s^4(\omega, z)}(r_{max})}{\overline{1/s^2(\omega, z)}^2(r_{max})}\right], \tag{16}$$

where as above the mean values are explicitly written to be evaluated at r_{max}. The condition of maximum fluence in Eq. (16) then leads to the inequality

$$\frac{\overline{1/s^4(\omega, z)}(r_{max})}{\overline{1/s^2(\omega, z)}^2(r_{max})} < \frac{|l| + 1}{|l|} \quad (17)$$

or, equivalently, to the inequality

$$\frac{\sigma^2_{1/s^2(\omega,z)}}{\overline{1/s^2(\omega, z)}^2} = \frac{\overline{1/s^4(\omega, z)} - \overline{1/s^2(\omega, z)}^2}{\overline{1/s^2(\omega, z)}^2} < \frac{1}{|l|}, \quad (18)$$

which is satisfied by any UFV at its maximum fluence at any propagation distance. In the equality (18) we have omitted again r_{max} in the mean values and variance to simplify the notation, but it should be understood from now on that they are evaluated at this radius. The inequality (18) is the main mathematical result of this paper, stating that the relative variance of the function of frequency $1/s^2(\omega, z)$ at the radius of maximum fluence of general UFVs is restricted by the upper bound on the right-hand side (rhs) of the inequality (18). The physical interpretation and consequences of this restriction are the purpose of the remainder of this paper.

Although the inequality (18) holds for arbitrarily short UFVs, i.e., also for subcycle pulses of arbitrary temporal shape and ultrabroadband spectrum, from now on we limit our considerations to pulses with at least one carrier oscillation as defined in [46], with a relatively narrow spectrum, as in the example of Fig. 1, and therefore with a physically meaningful carrier frequency. With this limitation the inequality (18) can be transformed under suitable approximations into useful inequalities involving the carrier frequency, the bandwidth, and the duration of the UFVs. This limitation is not a real limitation in practice, as current femtosecond laser sources do not go below single-cycle durations and are not expected to do so in the near future.

IV. RED AND BLUE FREQUENCY SHIFTS

To transform the inequality (18) into useful inequalities, we first investigate the actual carrier frequency of the oscillations of UFVs at their bright ring. It has been demonstrated in [34] that the carrier frequency of isodiffracting UFVs is not appreciably shifted from the source frequency ω_0, that is, $\bar{\omega} \simeq \omega_0$, in line with what happens to the fundamental isodiffracting pulsed Gaussian beam [40]. For UFVs with $g_0 \neq 0$ there are significant, but not large, blueshifts or redshifts of the carrier frequency, which are also similar to those of fundamental pulsed Gaussian beams of the same value of g_0 [44] and are substantially independent of the topological charge.

In Fig. 3(a) the carrier frequency $\bar{\omega}$ at the bright ring is represented for UFVs of the same topological charge and different values of g_0 versus propagation distance z about the focus for a single-cycle, approximately Gaussian source pulse $A(t)$ (see the caption for details). Starting in all cases with a carrier frequency $\bar{\omega} \simeq \omega_0$ far from the focus, the carrier frequency is increasingly redshifted approaching the focus for negative g_0 and increasingly blueshifted approaching the focus for positive g_0. As can be seen in Fig. 3(b) for $g_0 = 1$, the frequency shift at the focus does not appreciably depend on l and is approximately equal to that affecting the fundamental
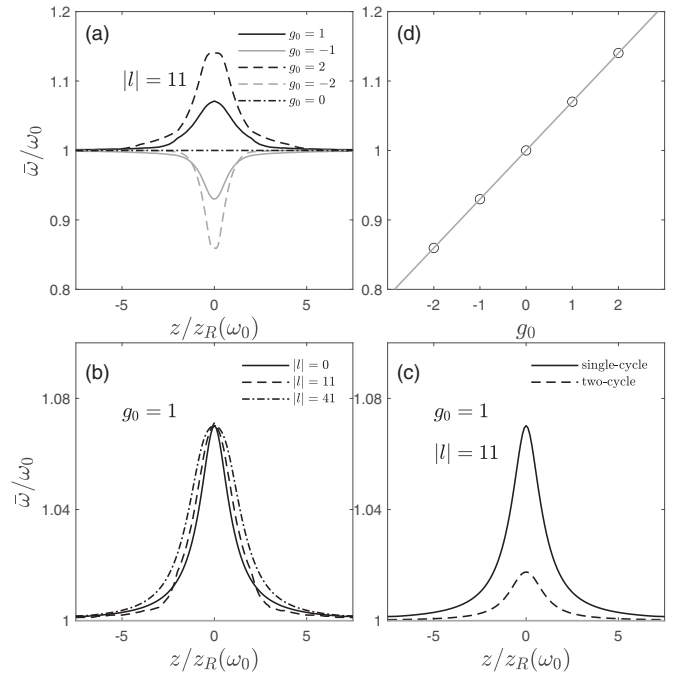

FIG. 3. Frequency shifts of UFVs at their bright ring. They are evaluated numerically with Eqs. (1), (2), and (10), with $Z_R(\omega) = Z_R(\omega_0)(\omega/\omega_0)^{g_0}$ and $\hat{A}(\omega) = (\omega/\omega_0)^{\alpha-1/2} \exp(-\alpha\omega/\omega_0)$ with $\alpha = 14.25$ (single-cycle pulse), except in (d), where $\alpha = 14.25$ for the single-cycle pulse and $\alpha = 57.11$ for the two-cycle pulse. The frequency shift is shown (a) for several values for g_0, (b) for different values of $|l|$, and (c) for different pulse durations, all of them as functions of propagation distance. (d) Frequency shifts at the focus $z = 0$ in (a) as a function of g_0, fitting approximately a straight line.

Gaussian beam of the same value of g_0. Off-focus the dependence of the frequency shift on the topological charge is also weak. For longer pulses, as for the two-cycle source pulse $A(t)$ in Fig. 3(c), the frequency shifts are much less pronounced and vanish in the monochromatic limit, as expected. Thus, the largest redshifts and blueshifts correspond to single-cycle input pulses at the focus and they fit the approximate linear variation with the g_0 factor shown in Fig. 3(d). These maximum frequency shifts are of course relevant in experiments, but for $|g_0| \leqslant 2$ do not exceed a relative variation of 15% with respect to the source carrier frequency, which justifies the approximations that will be made in the following section. Although particular power-exponential source spectra, corresponding to approximately Gaussian-shaped input pulses, are used in Fig. 3 (see the caption for details), we have observed in additional numerical simulations with other source spectra similar relative frequency shifts between 10% and 20%.

V. RESTRICTIONS TO THE BANDWIDTH AND DURATION

For $z_R(\omega)$ independent of frequency it can readily be seen from Eq. (4) that the inequality (18) reduces to the previously known inequality $\sigma_\omega/\bar{\omega} < 1/\sqrt{|l|}$ for isodiffracting UFVs that involves physically meaningful properties of the pulse at r_{max}. Taking into account that $\Delta\omega = 2\sigma_\omega$ and that $\Delta\omega\Delta t \geqslant 2$, the number of oscillations of isodiffracting UFVs satisfies $\bar{\omega}\Delta t \geqslant \sqrt{|l|}$ [30].

Similar, though approximate, restrictions involving the carrier frequency, bandwidth, and duration at r_{max} of general UFVs with at least one cycle can be obtained as follows. Using the approximate equality $\sigma_{f(\omega)}^2 \simeq [df(\omega)/d\omega|_{\bar{\omega}}]^2\sigma_\omega^2$ for $f(\omega) = 1/s^2(\omega, z)$ frequently used in statistics [56], evaluating the derivative as $df(\omega)/d\omega = -[1/s^4(\omega, z)]ds^2(\omega, z)/d\omega$ for convenience, and approaching $\overline{f(\omega)}$ in the denominator of (18) by the first-order Taylor series $\overline{f(\omega)} \simeq \overline{f(\bar{\omega}) + df(\omega)/d\omega|_{\bar{\omega}}(\omega - \bar{\omega})} = f(\bar{\omega})$, we obtain

$$\sigma_\omega < \frac{1}{\sqrt{|l|}} \left| \frac{s^2(\bar{\omega}, z)}{\frac{ds^2(\omega, z)}{d\omega}\Big|_{\bar{\omega}}} \right|. \tag{19}$$

Introducing the bandwidth $\Delta\omega = 2\sigma_\omega$ and using that $\Delta\omega\Delta t \geqslant 2$, the inequality (19) yields

$$\Delta t > \sqrt{|l|} \left| \frac{\frac{ds^2(\omega, z)}{d\omega}\Big|_{\bar{\omega}}}{s^2(\bar{\omega}, z)} \right|. \tag{20}$$

Explicit evaluation of the derivative yields the result

$$\frac{\sigma_\omega}{\bar{\omega}} < \frac{1}{\sqrt{|l|}} \frac{1}{\left| 1 + g(\bar{\omega})\frac{1 - z^2/z_R^2(\bar{\omega})}{1 + z^2/z_R^2(\bar{\omega})} \right|} \tag{21}$$

and

$$\bar{\omega}\Delta t > \sqrt{|l|} \left| 1 + g(\bar{\omega})\frac{1 - z^2/z_R^2(\bar{\omega})}{1 + z^2/z_R^2(\bar{\omega})} \right|, \tag{22}$$

where $g(\omega) = -\{[dz_R(\omega)/d\omega]/z_R(\omega)\}\omega$. The rhs of the inequality (22) imposes a lower bound on the number of oscillations of the pulse that is different at each propagation distance. Its evaluation is however difficult because one needs to know the functions of frequency $z_R(\omega)$ and $g(\omega)$ and then evaluate them at the carrier frequency $\bar{\omega}$ at the bright ring at each propagation distance. Experimentally this would require a careful characterization of the input source by determining $Z_R(\omega)$ as a function of frequency and measuring $\bar{\omega}$ at the bright ring at each selected distance. In a numerical simulation of an experiment, one would need to specify models of $\hat{A}(\omega)$ and $Z_R(\omega)$ of the input pulse, use Eqs. (10), compute the focused optical field with Eqs. (1) and (2), and extract the values of $\bar{\omega}$. As seen in the preceding section, the carrier frequency $\bar{\omega}$ at r_{max} may be redshifted or blueshifted with respect to the carrier frequency ω_0 of the source, but this shift does not exceed a relative value of 10–20% for the extreme case of single-cycle pulses, for $|g_0| \leqslant 2$, with any topological charge, and vanishes as the number of oscillations increases, regardless the particular choice of $\hat{A}(\omega)$ and $Z_R(\omega)$. Thus, we can transform the upper bound in (21) and the lower bound in (22) into approximate but much easier to evaluate upper and lower bounds by replacing $\bar{\omega}$ with the source frequency ω_0 on the rhs of the inequalities (21) and (22) to obtain

$$\frac{\sigma_\omega}{\bar{\omega}} < \frac{1}{\sqrt{|l|}} \frac{1}{\left| 1 + g_0\frac{1 - z^2/z_R^2(\omega_0)}{1 + z^2/z_R^2(\omega_0)} \right|} \tag{23}$$

and

$$\bar{\omega}\Delta t > \sqrt{|l|} \left| 1 + g_0\frac{1 - z^2/z_R^2(\omega_0)}{1 + z^2/z_R^2(\omega_0)} \right|, \tag{24}$$

whose right-hand sides are determined by standard properties of the source such as its carrier frequency ω_0 and Rayleigh distance $z_R(\omega_0) = f^2/Z_R(\omega_0)$ at the carrier frequency. The appearance of the g_0 factor underlines the need to measure it for the available laser source. The inequality (24), supplemented by the inequality (23), is the main practical result of this paper that imposes a z-dependent lower bound proportional to $\sqrt{|l|}$ on the number of oscillations at the bright ring of general UFVs and generalizes the z-independent lower bound $\sqrt{|l|}$ in the isodiffracting case.

It is possible to derive more intuitively the above results by examining more closely the spectral density

$$|\hat{E}(r, \omega, z)|^2 = \frac{f^2}{z_R^2(\omega)} \frac{s^2(\omega)}{s^2(\omega, z)} |\hat{A}(\omega)|^2 \left[\frac{2r^2}{s^2(\omega, z)} \right]^{|l|} e^{-2r^2/s^2(\omega, z)}. \tag{25}$$

Using the approximate equality $x^{2m}e^{-x^2} \simeq e^{-2(x - \sqrt{m})^2}(m/e)^m$, which becomes more accurate as the positive parameter m increases, the spectral density can be approximated by

$$|\hat{E}(r, \omega, z)|^2 \simeq \frac{f^2}{z_R^2(\omega)} \frac{s^2(\omega)}{s^2(\omega, z)} |\hat{A}(\omega)|^2 e^{-2[\sqrt{2}r/s(\omega, z) - \sqrt{|l|}]^2}, \tag{26}$$

where we have omitted the irrelevant $(m/e)^m$ factor. The first two factors are present also with $l = 0$ and induce carrier frequency shifts but do not significantly alter the bandwidth of the source spectrum $\hat{A}(\omega)$ in the same way as for pulsed Gaussian beams. The last factor is peculiar to UFVs and acts as a bandpass filter when $s(\omega, z)$ depends on frequency that limits the bandwidth and hence the duration. Approximating $1/s(\omega, z) \simeq 1/s(\omega_0, z) + d[1/s(\omega, z)]/d\omega|_{\bar{\omega}}(\omega - \bar{\omega})$, expressing for convenience the derivative as $d[1/s(\omega, z)]/d\omega = -[ds^2(\omega, z)/d\omega]/2s^3(\omega, z)$, and evaluating the spectral density at $r_{max}^2 = (|l|/2)[1/\overline{1/s^2(\omega, z)}] \simeq (|l|/2)s^2(\bar{\omega}, z)$, one arrives at

$$|\hat{E}(r_{max}, \omega, z)|^2 \simeq \frac{f^2}{z_R^2(\omega)} \frac{s^2(\omega)}{s^2(\omega, z)} |\hat{A}(\omega)|^2 e^{-(\omega - \bar{\omega})^2/2\sigma_G^2}, \tag{27}$$

with

$$\sigma_G = \frac{1}{\sqrt{|l|}} \left| \frac{s^2(\bar{\omega}, z)}{\frac{ds^2(\omega, z)}{d\omega}\Big|_{\bar{\omega}}} \right|. \tag{28}$$

As the product of $|\hat{A}(\omega)|^2$ and the last Gaussian factor in Eq. (27), the spectral density of the UFV at r_{max} cannot by wider than σ_G, that is, $\sigma_\omega < \sigma_G$, which is the same as the inequality (19), from which the remainder of the inequalities are derived.

The z-dependent lower bound to the number of oscillations at the bright ring of UFVs as given by the rhs of the inequality (24) is represented in Figs. 4(a) and 4(b) by means of solid curves for several values of g_0. For positive g_0 the lower bound in the focal region $[-z_R(\omega_0), z_R(\omega_0)]$ is above the bound $\sqrt{|l|}$ for isodiffracting UFVs, outside the focal region it is below $\sqrt{|l|}$, and at the edges $\pm z_R(\omega_0)$ of the focal region it equals $\sqrt{|l|}$. The opposite happens with negative values of g_0. For any $|g_0|$ the maximum lower bound is $(1 + |g_0|)\sqrt{|l|}$, reached at the focus for positive g_0 and far from the focus for negative g_0.
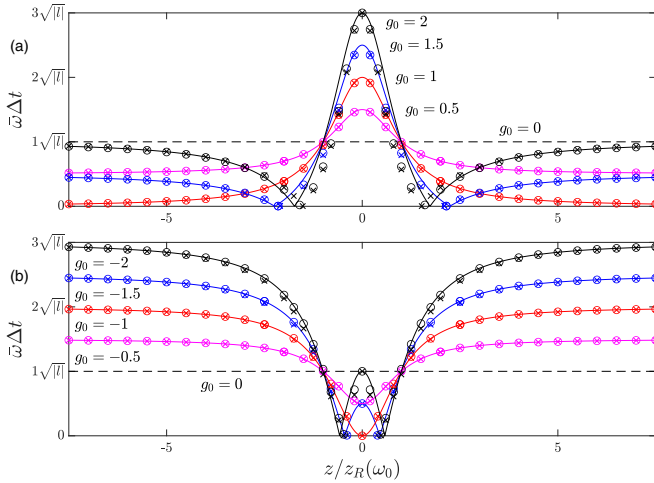
FIG. 4. Lower bound to the number of oscillations of UFVs as a function of propagation distance for several (a) positive and (b) negative values of the g_0 factor. The solid curves show the lower bound given by the rhs of the inequality (24). The symbols show the lower bound evaluated from the rhs of the inequality (22) using numerical simulations of the propagation with the source model $Z_R(\omega) = Z_R(\omega_0)(\omega/\omega_0)^{g_0}$ and spectra $\hat{A}(\omega)$ of single-cycle pulses of shapes $A(t) = [-i\alpha/(\omega_0 t - i\alpha)]^{\alpha+1/2}$, $\alpha = 14.25$, and $\omega_0 = 2.5$ rad/fs (open circles) and $A(t) = \mathrm{sinc}^2 t/T e^{-i\omega_0 t}$, $T = 3.9$ fs, and $\omega_0 = 2.5$ rad/fs (crosses).

Remarkably, for $|g_0| \geqslant 1$ there exist isolated axial positions

$$z_b = \pm\sqrt{\frac{g_0+1}{g_0-1}} z_R(\omega_0), \quad (29)$$

located outside the focal region for $g_0 \geqslant 1$ and within the focal region for $g_0 \leqslant -1$, where the lower bound vanishes and therefore there is no restriction on the minimum duration of the UFV. At z_b the lower bound disappears because $ds^2(\omega, z_b)/d\omega|_{\omega_0} = 0$, i.e., the Gaussian width of the monochromatic LG constituents is constant about the carrier frequency, which means, according to Eq. (27) with $\sigma_G = \infty$, that the spectral density is substantially the same as $|\hat{A}(\omega)|^2$ of the source, except for small changes associated with the frequency shifts. The absence of a lower bound when the Gaussian width is independent of frequency follows directly from the inequality (18) and therefore this conclusion is not limited to UFVs with at least one cycle. Indeed, if $s(\omega, z)$ is independent of ω at some axial location, the variance $\sigma^2_{1/s^2(\omega,z)}$ vanishes and the inequality (18) is automatically satisfied with any UFV bandwidth, duration, and topological charge. In practice, the absence of a lower bound means that the minimum duration of the UFV is only limited by the source spectrum $\hat{A}(\omega)$ to the duration of $A(t)$. This finding generalizes, to different positions z_b for different values of $|g_0| \geqslant 1$, the introductory example in Figs. 2(g)–2(i) with $z_b = \pm\infty$, i.e., at the focusing system in the Debye approximation, with $g_0 = 1$.

Figures 4(a) and 4(b) also serve to support the validity of (24) to approximate (22). The symbols in these figures represent the more precise lower bound provided by the rhs

of the inequality (22), which requires specifying particular models of $Z_R(\omega)$ and $\hat{A}(\omega)$, as detailed in the caption, computing the focused optical field and its actual carrier frequency $\bar{\omega}$ at the bright ring at each distance. In these figures circles and crosses correspond to source pulses of different shapes (Gaussian-like and sinc squared), all containing a single oscillation, in which case the frequency shifts are larger and then the discrepancies between (24) and (22) may be more pronounced. The deviations are however small and would indeed be inappreciable if, for instance, the symbols were evaluated using multiple-cycle input pulses. These simulations support that the rhs of (22) depends weakly on these fine details of the source, and therefore the lower bound on the number of oscillations can be accurately determined by the analytical formula of the rhs of (24), which is exclusively determined by the three parameters ω_0, $z_R(\omega_0)$, and g_0 pertaining to the source.

VI. PULSE SHAPE CHANGES UPON PROPAGATION AND WITH THE TOPOLOGICAL CHARGE, AND LOCALLY COMPRESSED STATES OF ORBITAL ANGULAR MOMENTUM

The change in the number of oscillations of the UFV upon propagation, as in the introductory example in Figs. 2(g)–2(i), can be explained as a consequence of the existence of the z-varying lower bound in the inequality (24).

The solid black and gray curves in Fig. 5(a) represent $\bar{\omega}\Delta t$ at the bright ring of the UFV as a function of propagation distance for the input UFVs $E_L(r, t)e^{il\varphi} = A(t)[\sqrt{2}r/S(\omega_0)]^{|l|} e^{-r^2/S(\omega_0)^2} e^{il\varphi}$ with $g_0 = 1$ because $Z_R(\omega)$ is such that $S(\omega) = S(\omega_0)$ is independent of frequency. The source spectra $\hat{A}(\omega)$ are chosen to represent Gaussian-like pulses $A(t)$ of one, two, and three oscillations, whose values of $\omega_0 \Delta t$ are represented as dash-dotted blue lines for reference. As can be seen, the number of oscillations of the respective UFVs (black, dark gray, and light gray) remains at any propagation distance above the lower bound, represented as a red curve. The lower bound acts as a kind of effective barrier that requires a significant broadening of the input single-cycle and two-cycle UFVs. A similar situation, but reversing the focal region and far field, is given with $g_0 = -1$, as illustrated in Fig. 5(b). The input UFV is given by Eqs. (6) and (7) with $Z_R(\omega)$ such that $\Theta(\omega) = \Theta(\omega_0)$, and hence $s(\omega) = s(\omega_0)$ at the focus, is independent of frequency and with $\hat{A}(\omega)$ such that $A(t)$ comprises one, two, and three oscillations, as above. Regardless of how low $\omega_0 \Delta t$ of the source pulse is (dash-dotted lines), the number of oscillations of the synthesized UFV on the focusing system and as it is directed towards the focus (black, dark gray, and light gray curves) is above the lower bound (red curve), and it is only when the lower bound diminishes in the focal region that this particular UFV compresses to a duration also allowed by the lower bound in this region and always above or equal to the duration of $A(t)$. For longer input durations, such as the three-cycle UFV in both examples, these pulse shape changes during propagation are less and less pronounced.

The proportionality of the lower bound to $\sqrt{|l|}$ entails an increase of the number of oscillations with $|l|$ at any particular location z, in the same way as for isodiffracting UFVs [30].
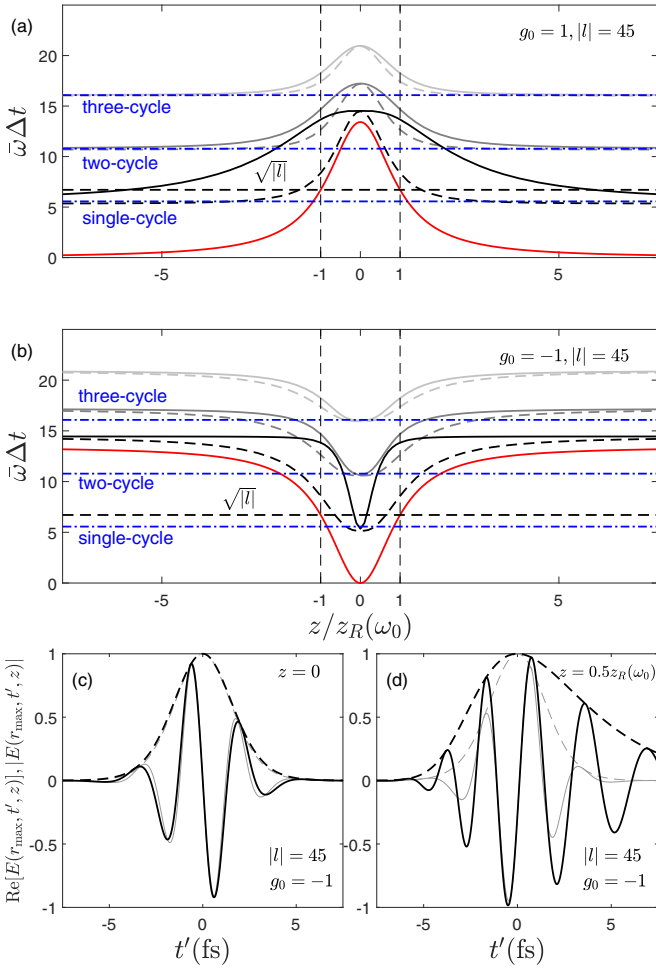
FIG. 5. (a) and (b) Black and gray solid curves show the change of the number of oscillations $\bar{\omega}\Delta t$ at the bright ring of UFVs during propagation evaluated numerically with Eqs. (1), (2), and (10), with $Z_R(\omega) = Z_R(\omega_0)(\omega/\omega_0)^{g_0}$ and $\hat{A}(\omega) = (\omega/\omega_0)^{\alpha-1/2}\exp(-\alpha\omega/\omega_0)$ with $\alpha = 14.25$ (single-cycle pulse), $\alpha = 57.11$ (two-cycle pulse), and $\alpha = 128.30$ (three cycle pulse) and $|l| = 45$. In (a) $g_0 = 1$ and in (b) $g_0 = -1$. The solid red curve shows the lower bound in the inequality (24). The dashed curves show the number of oscillations $\bar{\omega}\Delta t$ evaluated with transform-limited durations $\Delta t = 2/\Delta\omega$. The dash-dotted horizontal blue lines show $\bar{\omega}\Delta t$ for the source pulses. The dashed horizontal line shows the isodiffracting lower bound $\sqrt{|l|}$. (c) and (d) Pulse shapes at the bright ring at the indicated distances (black curves) of the source single-cycle pulse (gray curves).

For the same input UFVs as in Figs. 5(a) and 5(b), the number of oscillations and the lower bound $\sqrt{l}(1 + |g_0|)$ are represented in Fig. 6(a) as functions of $|l|$ at the focal plane for $g_0 = 1$ and at the far field for $g_0 = -1$. The existence of a lower bound monotonically increasing with $|l|$ at each particular location z imposes the increase of the number of oscillations with increasing magnitude of the imprinted topological charge with respect to those of $A(t)$. As the frequency shifts are small, the envelopes shown in Fig. 6(b) are increasingly broadened at the focus for $g_0 = 1$ and at the far field for $g_0 = -1$ (they are identical) when increasing $|l|$ compared to the envelope of $A(t)$. Interestingly, this effect at an important location such as the focal plane is more pronounced than for isodiffracting
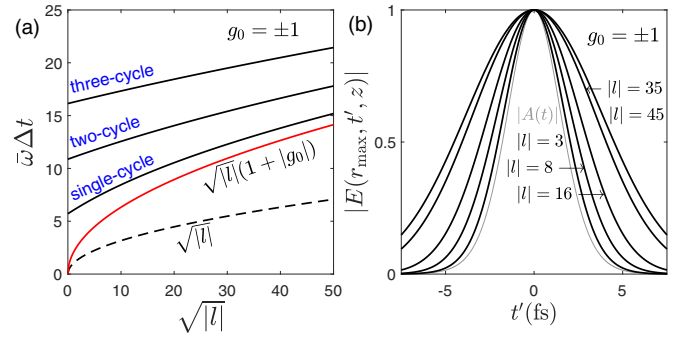

FIG. 6. (a) Number of oscillations $\bar{\omega}\Delta t$ at the bright ring at the focal plane for $g_0 = 1$ and at the far field for $g_0 = -1$ with the same input conditions as in Fig. 5 as a function of the imprinted topological charge. The red curve is the lower bound in the inequality (24) and the dashed black curve the lower bound for isodiffracting UFVs. (b) Broadened amplitudes for various values of $|l|$ at the focal plane for $g_0 = 1$ and at the far field for $g_0 = -1$, compared to the source amplitude.

UFVs. Figure 6(a) also evidences that the effect of broadening with the magnitude of the topological charge is particularly enhanced and observable with current sources emitting pulses of duration between one and two cycles and with imprinted topological charges below ten, e.g., a single-cycle source pulse with $g_0 = 1$ would acquire an additional half a cycle at the focus if it is forced to carry topological charge $|l| = 10$. On the contrary, the slope of the black curves in Fig. 6(a) decreases with increasing number of cycles, meaning that broadening with increasing topological charge is gradually less pronounced in the multicycle regime and vanishes in the monochromatic limit.

The above two examples also illustrate what we will refer to as locally compressed states of OAM or UFVs, understood as UFVs whose number of oscillations is locally below the lower bound $\sqrt{|l|}$ for isodiffracting UFVs, represented in Figs. 5(a) and 5(b) as dashed black lines. Indeed, the bound $\sqrt{|l|}$ for isodiffracting UFVs continues to play a prominent role for general UFVs with $g_0 \neq 0$ with axially varying pulse shape. Note that for $0 < |g_0| \leqslant 1$, the mean value of the minimum and maximum values of the lower bound, $\sqrt{|l|}(1 - |g_0|)$ and $\sqrt{|l|}(1 + |g_0|)$, respectively, along the propagation is just the isodiffracting value $\sqrt{|l|}$. Thus, as in Fig. 5(a) for a source with $g_0 = 1$ and single-cycle $A(t)$, the UFV at the far field with $\bar{\omega}\Delta t < \sqrt{|l|}$ (black dashed line) can be regarded as such a compressed UFV because it necessarily increases its number of oscillations to a value $\bar{\omega}\Delta t > \sqrt{|l|}$. Conversely, for the source with $g_0 = -1$ and single-cycle $A(t)$, it is possible to create, as in Fig. 5(b), an UFV with $\bar{\omega}\Delta t < \sqrt{|l|}$ in the focal region, but it immediately broadens to $\bar{\omega}\Delta t > \sqrt{|l|}$. These locally compressed UFVs are located about the minimum of the lower bound in each case, but can only be implemented in practice, as justified below, when the minimum lower bound $\sqrt{|l|}(1 - |g_0|)$ is either in the far field (focusing system) or at the focus i.e., with sources with $|g_0| \leqslant 1$, and can be optimally implemented with $g_0 = \pm 1$ because the minimum lower bounds vanish. In these two cases, the value of $\bar{\omega}\Delta t$ at the far field or at the focus can reach its minimum practical value for the given source spectrum, as in Figs. 5(a) and 5(b),
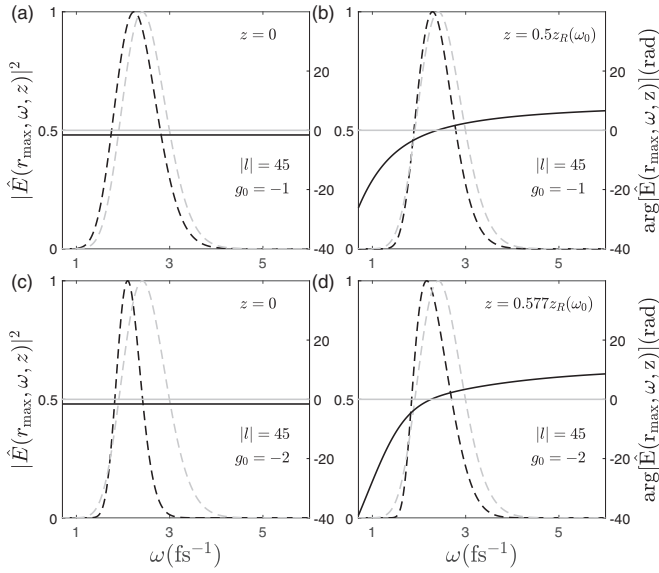
FIG. 7. From (a) to (d) the black solid and dashed curves represent the spectral phase and density of the pulses in the respective pulses in Figs. 5(c), 5(d), 8(b), and 8(c). The gray solid and dashed curves are the same quantities for the single-cycle source pulse $A(t)$. All spectral densities are normalized to unity and the absolute value of the spectral phase is arbitrary; only its variation is relevant.

where the pulse shape at the bright ring is almost identical to $A(t)$, except for the small redshift at the focus, as observed in Fig. 5(c).

In principle, these compressed states of OAM could survive, as allowed by the lower bound, the whole far field $|z| > z_R(\omega_0)$ or the whole focal region $|z| < z_R(\omega_0)$. However, as a general feature, they are much more localized axially, e.g., they exist only in a fraction of the far field in Fig. 5(a) or in a fraction of the focal region in Fig. 5(b). This limitation originates from the nonlinear spectral phases acquired during propagation when the Rayleigh range depends on frequency, which have therefore a dispersive effect that broadens and distort the pulse shape. These nonlinear spectral phases are introduced by the ω-dependent Gouy phase $-(|l| + 1) \tan^{-1}[z/z_R(\omega)]$, which is strongly enhanced for large $|l|$, and by the phases $\omega r_{\max}^2/2cR(\omega, z)$ due to ω-dependent wave fronts, or wave-front mismatch, as the UFV approaches the focal region from the outside or is immediately off-focus. Figures 7(a) and 7(b) showing the spectral phases and densities of the pulses in Fig. 5(c) at the focus and Fig. 5(d) at one-half the Rayleigh distance evidences that the spectral densities are similar but the latter is broadened and distorted because of the nonlinear spectral phases. The limiting effect of these dispersions on the axial length of the compressed state is also clear by comparing the pulse durations, depicted as the black curves and the dashed curves in Figs. 5(a) and 5(b). These dashed curves represent the number of oscillations that the pulse would have without Gouy's phase and wave-front mismatch dispersions, evaluated as if the pulse would remain almost Gaussian shaped with uniform spectral phases from the relation $\bar{\omega} \Delta t \simeq \bar{\omega} 2/\Delta \omega$, where $\Delta \omega$ is the computed bandwidth. This comparison evidences that the length of the compressed states is reduced from almost
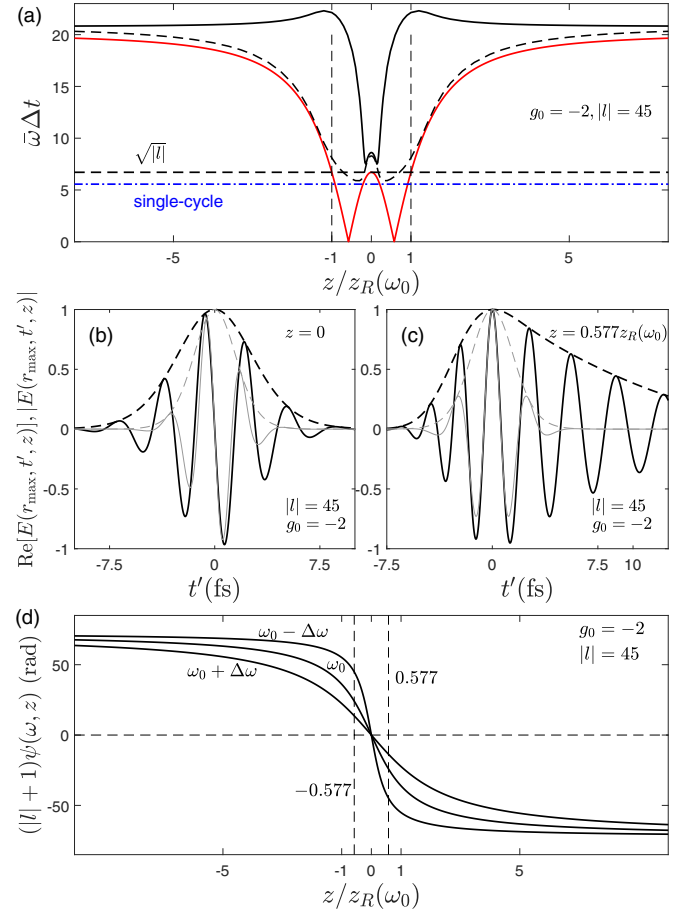

FIG. 8. (a) The black curve shows the change of the number of oscillations $\bar{\omega} \Delta t$ at the bright ring of UFVs during propagation evaluated numerically with Eqs. (1), (2), and (10), with $Z_R(\omega) = Z_R(\omega_0)(\omega/\omega_0)^{g_0}$, $g_0 = -2$, $\hat{A}(\omega) = (\omega/\omega_0)^{\alpha-1/2} \exp(-\alpha \omega/\omega_0)$, $\alpha = 14.25$ (single-cycle pulse), and $|l| = 45$. The solid red curve shows the lower bound in the inequality (24). The dashed gray curve shows the number of oscillations $\bar{\omega} \Delta t$ evaluated with transform-limited durations $\Delta t = 2/\Delta \omega$. The dash-dotted horizontal blue line shows $\bar{\omega} \Delta t$ for the source pulse. The dashed horizontal line shows the isodiffracting lower bound $\sqrt{|l|}$. (b) and (c) Pulse shapes at the bright ring at the indicated distances (black curves) of the source single-cycle pulse (gray curves). (d) Gouy's phases of the monochromatic LG beams of the source carrier frequency ω_0 and of frequencies $\omega_0 + \Delta \omega$ and $\omega_0 - \Delta \omega$ at the edge of the source spectrum.

the entire far field and almost the entire focal region to small fractions of them by the effect of these dispersions in the respective cases of $g_0 = 1$ and $g_0 = -1$.

With sources characterized by $|g_0| > 1$, such as that used in [47], the situation is worse for the purpose of focusing to an as short as possible pulse in a compressed UFV. First, the mean value of the maximum and minimum numbers of oscillations along the propagation is $\sqrt{|l|}(1 + |g_0|)/2$, above the isodiffracting lower bound $\sqrt{|l|}$. Second, the points z_b where the lower bound vanishes are not at infinity but somewhere outside the focal region for $g_0 > 1$ and not at the focus but somewhere in the focal region for $g_0 < -1$, as illustrated in Fig. 8. The possible compressed states located

about z_b are not so because of the nonlinear spectral phases introduced by Gouy's phase and wave-front mismatch dispersions, which make the pulses broaden and distort. With the same input conditions as in Fig. 5(a) except that $g_0 = -2$, the number of oscillations of the UFV (black curve) is seen in Fig. 8(a) to be enormously increased in the focusing system while it is directed towards the focus compared to the source single-cycle pulse (dash-dotted blue line), as imposed by the lower bound (red curve). Removing artificially Gouy's phase and wave-front mismatch dispersions, the UFV would focus about $z_b = 0.577 z_R(\omega_0)$ into a compressed state (dashed gray curve) with the number of oscillations below $\sqrt{|l|}$ (dashed horizontal line). The pulse at the focus in Fig. 8(b) is significantly broadened compared to $A(t)$, as imposed by the lower bound; the pulse shape at z_b in Fig. 8(c) is even more broadened and distorted as a result of dispersion. The spectral phases and densities of these two pulses are depicted in Figs. 7(c) and 7(d) to evidence that with similar bandwidths the latter is substantially longer than the former because of the nonuniform spectral phases. Figure 8(d) helps to visualize Gouy's phase dispersion, i.e., the different values of Gouy's phase for different spectral components, which is the main origin of the distortion for high topological charges.

To conclude, it should be clear that reaching the minimum number of oscillations of the source pulse $A(t)$, i.e., the blue dash-dotted line in Fig. 8(a), is not impossible, because the lower bound actually vanishes at z_b, but only very difficult in practice. It would require measuring the nonuniform spectral phases of the UFV at (r_{max}, z_b) and precompensating for them prior to the focusing system, namely, and introducing spectral phases $(|l| + 1) \tan^{-1}[z_b/z_R(\omega)]$ opposite to Gouy's phase and $-\omega r_{max}^2/2cR(\omega, z_b)$ opposite to the front mismatch for each particular frequency. This precompensation is however specific to the particular point (r_{max}, z_b) and the resulting UFV would be a locally compressed state of OAM about z_b.

VII. CONCLUSION

We have conducted an analytical and numerical study of the free-space propagation features of general Laguerre-Gauss ultrafast vortices similar to those generated in experiments from femtosecond laser sources, whose Rayleigh distance is generally spectrally varying, as characterized by the g_0 factor. The first conclusion to keep in mind is that the simple view of an approximately invariable pulse envelope modulated in space by a diffracting Laguerre-Gauss beam, which is widely taken for granted but is only acceptable for few-cycle Gaussian beams with any reasonable g_0 factor [40,44], is far from describing the actual propagation characteristics of ultrafast vortices. Ultrafast vortices experience similar small frequency shifts at their bright ring as ultrafast Gaussian beams of the same value of g_0 at their center, but additionally they experience nontrivial changes in the pulse shape that depend on $|l|$ and g_0 during propagation, these changes being more pronounced as $|l|$ and $|g_0|$ are higher and as the ultrafast vortex is shorter.

Instead of studying in detail the characteristics of particular models of ultrafast vortices, we have extracted general laws

underlying the behavior of all of them that explain the above phenomena. We have found an upper bound to the bandwidth relative to the carrier frequency and a lower bound to the duration relative to the carrier period, i.e., to the number of oscillations, of the pulse at the most energetic ring, bounds that are satisfied by all synthesizable ultrafast vortices in experiments and that generalize the bounds recently described for isodiffracting ultrafast vortices [30]. The lower bound on the number of oscillations, as given by the right-hand side of the inequality (24), remains proportional to the lower bound $\sqrt{|l|}$ for isodiffracting ultrafast vortices, with axial modulations whose locations depend on g_0 and whose maximum and minimum average value is $\sqrt{|l|}$ for $|g_0| \leqslant 1$ or the higher average value $\sqrt{|l|}(1 + |g_0|)$ for $|g_0| > 1$.

The existence of this lower bound explains the increase of the duration with increasing $|l|$ of the synthesized ultrafast vortex from the duration expected with the available bandwidth, this broadening being similar to that already described for isodiffracting ultrafast vortices [31], and the axial modulation of the lower bound explains the changes in the duration of the vortex upon propagation. With current femtosecond laser sources emitting pulses of duration between one and two cycles, these effects are very pronounced with topological charges of several tens and still clearly observable below ten.

The lower bound $\sqrt{|l|}$ for isodiffracting ultrafast vortices can be violated locally in what we have called locally compressed states of orbital angular momentum about the axial minima of the lower bound, but these states can be implemented in practice only with sources with $0 < g_0 \leqslant 1$ at the far field or with sources with $-1 \leqslant g_0 < 0$ at the focal plane. The optimum condition to create a compressed state of orbital angular momentum in the focal plane is a source with $g_0 = -1$ because the minimum lower bound vanishes at this plane. The term "locally" stresses here that these states can only survive a small fraction of the Rayleigh distance because of Gouy's phase and wave-front mismatch dispersions with $g_0 \neq 0$ that strongly broaden and distort the pulse immediately off-focus.

We have focused our interest on the effects of orbital angular momentum on pulse shape at the radius where the pulse energy is maximum because of its relevance in experiments and applications. Similar effects are expected at the radius of maximum pulse peak intensity because it is usually close to or coincides with the former, as described in [33]. Also, in the vicinity of the vortex center, a pronounced blueshift increasing with topological charge is expected, as described in [34]. A detailed description of these other coupling effects deserves a separate study.

Recent research has revealed the dependence on the g_0 factor, characterizing the variation with frequency of the beam parameters, of a variety of carrier-envelope-phase sensitive phenomena of interaction of few-cycle pulses with matter, such as electron acceleration with radially polarized pulses, high-harmonic and attosecond pulse generation, and electron photoemission from few-cycle pulses without orbital angular momentum [47–49]. Given the nontrivial dependence of the propagation features of ultrafast vortices with the topological charge l and the g_0 factor, this work stresses further the importance of measuring the g_0 factor of the femtosecond

laser source in use for an adequate design and interpretation of experiments involving few-cycle pulses with orbital angular momentum and for improvement and control of their applications.

[1] K. Bezuhanov, A. Dreischuh, G. G. Paulus, M. G. Schätzel, and H. Walther, Vortices in femtosecond laser fields, Opt. Lett. **29**, 1942 (2004).

[2] I. G. Mariyenko, J. Strohaber, and C. J. G. J. Uiterwaal, Creation of optical vortices in femtosecond pulses, Opt. Express **13**, 7599 (2005).

[3] K. Bezuhanov, A. Dreischuh, G. Paulus, M. G. Schätzel, H. Walther, D. Neshev, W. Krolikowski, and Y. Kivshar, Spatial phase dislocations in femtosecond laser pulses, J. Opt. Soc. Am. B **23**, 26 (2006).

[4] I. Zeylikovich, H. I. Sztul, V. Kartazaev, T. Le, and R. R. Alfano, Ultrashort Laguerre-Gaussian pulses with angular and group velocity dispersion compensation, Opt. Lett. **32**, 2025 (2007).

[5] Y. Tokizane, K. Oka, and R. Morita, Supercontinuum optical vortex pulse generation without spatial or topological-charge dispersion, Opt. Express **17**, 14517 (2009).

[6] V. G. Shvedov, C. Hnatovsky, W. Krolikowski, and A. V. Rode, Efficient beam converter for the generation of high-power femtosecond vortices, Opt. Lett. **35**, 2660 (2010).

[7] A. Richter, M. Bock, J. Jahns, and R. Grunwald, in Complex Light and Optical Forces IV, edited by E. J. Galvez, D. L. Andrews, and J. Glückstad, SPIE Proc. **7613** 761308 (2010).

[8] K. Yamane, Y. Toda, and R. Morita, Ultrashort optical-vortex pulse generation in few-cycle regime, Opt. Express **20**, 18986 (2012).

[9] M. Bock, J. Jahns, and R. Grunwald, Few-cycle high-contrast vortex pulses, Opt. Lett. **37**, 3804 (2012).

[10] N. A. Chaitanya, M. V. Jabir, and G. K. Samanta, Efficient nonlinear generation of high power, higher order, ultrafast "perfect" vortices in green, Opt. Lett. **41**, 1348 (2016).

[11] M. Miranda, M. Kotur, P. Rudawski, C. Guo, A. Harth, A. L'Huillier, and C. L. Arnold, Spatiotemporal characterization of ultrashort optical vortex pulses, J. Mod. Opt. **64**, S1 (2017).

[12] R. Grunwald, T. Elsaesser, and M. Bock, Spatio-temporal coherence mapping of few-cycle vortex pulses, Sci. Rep. **4**, 7148 (2015).

[13] D. N. Naik, N. A. Saad, D. N. Rao, and N. K. Viswanathan, Ultrashort vortex from a Gaussian pulse—An achromatic-interferometric approach, Sci. Rep. **7**, 2395 (2017).

[14] C. Hernández-García, A. Picón, J. San Román, and L. Plaja, Attosecond Extreme Ultraviolet Vortices from High-Order Harmonic Generation, Phys. Rev. Lett. **111**, 083602 (2013).

[15] G. Gariepy, J. Leach, K. T. Kim, T. J. Hammond, E. Frumker, R. W. Boyd, and P. B. Corkum, Creating High-Harmonic Beams with Controlled Orbital Angular Momentum, Phys. Rev. Lett. **113**, 153901 (2014).

[16] L. Rego, J. S. Román, A. Picón, L. Plaja, and C. Hernández-García, Nonperturbative Twist in the Generation of Extreme-Ultraviolet Vortex Beams, Phys. Rev. Lett. **117**, 163202 (2016).

[17] R. Gńeaux, A. Camper, T. Auguste, O. Gobert, J. Caillat, R. Taïeb, and T. Ruchon, Synthesis and characterization of attosecond light vortices in the extreme ultraviolet, Nat. Commun. **7**, 12583 (2016).

[18] D. Gauthier, P. Rebernik Ribic, G. Adhikary, A. Camper, C. Chappuis, R. Cucini, L. F. DiMauro, G. Dovillaire, F. Frassetto, R. Géneaux, P. Miotti, L. Poletto, B. Ressel, C. Spezzani, M. Stupar, T. Ruchon, and G. De Ninno, Tunable orbital angular momentum in high-harmonic generation, Nat. Commun. **8**, 14971 (2017).

[19] F. Kong, C. Zhang, F. Bouchard, Z. Li, G. G. Brown, D. H. Ko, T. J. Hammond, L. Arissian, R. W. Boyd, E. Karimi, and P. B. Corkum, Controlling the orbital angular momentum of high harmonic vortices, Nat. Commun. **8**, 14970 (2017).

[20] C. Hernández-García, A twist in coherent X-rays, Nat. Phys. **13**, 327 (2017).

[21] K. M. Dorney, L. Rego, N. J. Brooks, J. San Román, C.-T. Liao, J. L. Ellis, D. Zusin, C. Gentry, Q. L. Nguyen, J. M. Shaw, A. Picón, L. Plaja, H. C. Kapteyn, M. M. Murnane, and C. Hernández-García, Controlling the polarization and vortex charge of attosecond high-harmonic beams via simultaneous spin-orbit momentum conservation, Nat. Photon. **13**, 123 (2019).

[22] A. Turpin, L. Rego, A. Picón, J. San Román, and C. Hernández-García, Extreme ultraviolet fractional orbital angular momentum beams from high harmonic generation, Sci. Rep. **7**, 43888 (2017).

[23] L. Rego *et al.*, Generation of extreme-ultraviolet beams with time-varying orbital angular momentum, Science **364**, 1253 (2019).

[24] W. Zhang and L. Chen, High-harmonic-generation-inspired preparation of optical vortex arrays with arbitrary-order topological charges, Chin. Opt. Lett. **16**, 030501 (2018).

[25] S. Feng and H. G. Winful, Higher-order transverse modes of ultrashort isodiffracting pulses, Phys. Rev. E **63**, 046602 (2001).

[26] G. Pariente and F. Quéré, Spatio-temporal light springs: Extended encoding of orbital angular momentum in ultrashort pulses, Opt. Lett. **40**, 2037 (2015).

[27] J. Lekner, Angular momentum of electromagnetic pulses, J. Opt. A: Pure Appl. Opt. **6**, S128 (2004).

[28] J. Nie, G. Liu, and R. Zhang, Propagation and spatiotemporal coupling characteristics of ultra-short Gaussian vortex pulse, Opt. Laser Technol. **101**, 446 (2018).

[29] J. Nie, Q. Xiao, G. Liu, and R. Zhang, Propagation characteristics of ultra-short Gaussian vortex beams, Optik **141**, 99 (2017).

[30] M. A. Porras, Upper Bound to the Orbital Angular Momentum Carried by an Ultrashort Pulse, Phys. Rev. Lett. **122**, 123904 (2019).

[31] M. A. Porras, Effects of orbital angular momentum on few-cycle and sub-cycle pulse shapes: Coupling between the temporal and angular momentum degrees of freedom, Opt. Lett. **44**, 2538 (2019).

[32] M. A. Porras, Attosecond helical pulses, Phys. Rev. A **100**, 033826 (2019).

[33] M. A. Porras, Effects of the coupling between the orbital angular momentum and the temporal degrees of freedom in the most intense ring of ultrafast vortices, Appl. Sci. **10**, 1957 (2020).

[34] M. A. Porras and C. Conti, Couplings between the temporal and orbital angular momentum degrees of freedom in ultrafast optical vortices, Phys. Rev. A **101**, 063803 (2020).

[35] M. Ornigotti, C. Conti, and A. Szameit, Effect of Orbital Angular Momentum on Nondiffracting Ultrashort Optical Pulses, Phys. Rev. Lett. **115**, 100401 (2015).

[36] M. Ornigotti, C. Conti, and A. Szameit, Universal form of the carrier frequency of scalar and vector paraxial X waves with orbital angular momentum and arbitrary frequency spectrum, Phys. Rev. A **92**, 043801 (2015).

[37] S. Akturk, X. Gu, P. Bowlan, and R. Trebino, Spatio-temporal couplings in ultrashort laser pulses, J. Opt. **12**, 093001 (2010).

[38] C. J. R. Sheppard and X. Gan, Free-space propagation of femto-second light pulses, Opt. Commun. **133**, 1 (1997).

[39] A. E. Kaplan, Diffraction-induced transformation of near-cycle and subcycle pulses, J. Opt. Soc. Am. B **15**, 951 (1998).

[40] M. A. Porras, Ultrashort pulsed Gaussian light beams, Phys. Rev. E **58**, 1086 (1998).

[41] M. A. Porras, Nonsinusoidal few-cycle pulsed light beams in free space, J. Opt. Soc. Am. B **16**, 1468 (1999).

[42] M. A. Porras, Diffraction effects in few-cycle optical pulses, Phys. Rev. E **65**, 026606 (2002).

[43] M. A. Porras, R. Borghi, and M. Santarsiero, Few-optical-cycle Bessel-Gauss pulsed beams in free space, Phys. Rev. E **62**, 5729 (2000).

[44] M. A. Porras, Characterization of the electric field of focused pulsed Gaussian beams for phase-sensitive interactions with matter, Opt. Lett. **34**, 1546 (2009).

[45] E. Karimi, C. Altucci, V. Tosa, R. Velotta, and L. Marrucci, Influence of generalized focusing of few-cycle Gaussian pulses in attosecond pulse generation, Opt. Express **21**, 24991 (2013).

[46] T. Brabec and F. Krausz, Nonlinear Optical Pulse Propagation in the Single-Cycle Regime, Phys. Rev. Lett. **78**, 3282 (1997).

[47] D. Hoff, M. Kruger, L. Maisenbacher, A. M. Sayler, G. G. Paulus, and P. Hommelhoff, Tracing the phase of focused broad-band laser pulses, Nat. Phys. **133**, 947 (2017).

[48] Y. Zhang, D. Zille, D. Hoff, P. Wustelt, D. Würzler, M. Möller, A. M. Sayler, and G. G. Paulus, Observing the Importance of the Phase-Volume Effect for Few-Cycle Light-Matter Interactions, Phys. Rev. Lett. **124**, 133202 (2020).

[49] S. W. Jolly, On the importance of frequency-dependent beam parameters for vacuum acceleration with few-cycle radially-polarized laser beams, Opt. Lett. **45**, 3865 (2020).

[50] T. Tritschler, K. D. Hof, M. W. Klein, and M. Wegener, Variation of the carrier-envelope phase of few-cycle laser pulses owing to the Gouy phase: A solid-state-based measurement, Opt. Lett. **30**, 753 (2005).

[51] F. Lindner, G. G. Paulus, H. Walther, A. Baltuska, E. Goulielmakis, M. Lezius, and F. Krausz, Gouy Phase Shift for Few-Cycle Laser Pulses, Phys. Rev. Lett. **92**, 113001 (2004).

[52] M. A. Porras, Z. L. Horváth, and B. Major, Three-dimensional carrier-envelope-phase map of focused few-cycle pulsed Gaussian beams, Phys. Rev. A **98**, 063819 (2018).

[53] M. Born and E. Wolf, *Principles of Optics* (Pergamon Press, Oxford, 1975).

[54] J. P. Taché, Derivation of ABCD law for Laguerre-Gaussian beams, Appl. Opt. **26**, 2698 (1987).

[55] C. F. R. Caron and R. M. Potvliege, Free-space propagation of ultrashort pulses: Space-time couplings in Gaussian pulse beams, J. Mod. Opt. **46**, 1881 (1999).

[56] J. M. Ver Hoef, Who invented the delta method? Am. Stat. **66**, 124 (2012).